Thin-Film Lithium Niobate Acoustic Delay Line Oscillators

Li, Ming Huang; Lu, Ruochen; Manzaneque, Tomas; Gong, Songbin

DOI
10.1109/MEMS46641.2020.9056259

Publication date
2020

Document Version
Accepted author manuscript

Published in
Proceedings of the 33rd IEEE International Conference on Micro Electro Mechanical Systems, MEMS 2020

THIN-FILM LITHIUM NIOBATE ACOUSTIC DELAY LINE OSCILLATORS

Ming-Huang Li[1,2], Ruochen Lu[1], Tomas Manzaneque[3], and Songbin Gong[1]
[1]University of Illinois at Urbana–Champaign, Urbana, Illinois, USA
[2]National Tsing Hua University, Hsinchu, TAIWAN
[3]Delft University of Technology, Delft, The Netherlands

ABSTRACT

In this work, thin-film lithium niobate ($LiNbO_3$) acoustic delay line (ADL) based oscillators are experimentally investigated for the first time for the application of single-mode oscillators and frequency comb generation. The design space for the ADL-based oscillator is first analyzed, illustrating that the key to low phase noise lies in high center frequency (f_o), large delay (τ_G), and low insertion loss (IL) of the delay. Therefore, two self-sustained oscillators employing low noise amplifiers (LNA) and a low IL, long delay (f_o = 157MHz, IL = 2.9 dB, τ_G = 200 – 440ns) SH_0 mode ADLs are designed for a case study. The two SH_0 ADL oscillators show measured phase noise of -109 dBc/Hz and -127 dBc/Hz at 10-kHz offset while consuming 16 mA and 48 mA supply currents, respectively. Although the carrier power of the proposed oscillator is lower than published state-of-the-art ADL oscillators, competitive phase noise performance is still attained thanks to the low IL. Finally, frequency comb generation is also demonstrated with the same delay line and a commercial RF feedback amplifier, showing a comb spacing of 3.4 MHz that matches the open-loop characterization.

KEYWORDS

MEMS, lithium niobate, acoustic delay lines, oscillator, piezoelectric transducers, phase noise.

INTRODUCTION

Acoustic delay lines (ADL) are a useful function block for a wide verity of applications, such as chemical sensors [1], nonreciprocal components [2], frequency references [3], RF filters [4], and frequency-agile radars [5]. Thanks to the recent advances on microelectromechanical systems (MEMS) technologies, high-performance MEMS plate wave ADLs based on lithium niobate ($LiNbO_3$) [6]-[10], aluminum nitride (AlN) [11], and gallium nitride (GaN) [12][13] have been explored. Among the piezoelectric materials investigated so far, $LiNbO_3$ is the most promising for plate wave ADL as it provides larger electromechanical coupling (k^2) and reflectivity (Γ) than conventional surface acoustic wave (SAW) ADLs. The exceptional k^2 and various available modes in $LiNbO_3$ can result in wide bandwidth (BW), low insertion loss (IL), and high frequency (f_o) ADL over a wide range of time delay (τ_G). As evidence, $LiNbO_3$ delay lines have recently been demonstrated at GHz frequenies with sub-10 dB IL and τ_G up to 900 ns using both the fundamental symmetric Lamb wave (S_0) [7] and fundamental shear horizontal plate wave (SH_0) [14]. Low loss, long delay, high frequency, and wideband shown in these ADLs are especially beneficial to realizing low phase noise and power-efficient designs as either a single-mode RF oscillator [12] or a comb frequency generator [15].

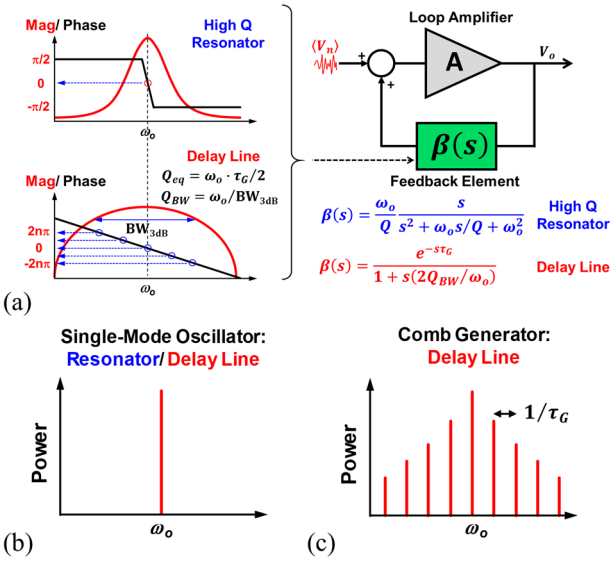

Figure 1: (a) LTI model representation for general oscillators employing a high-Q resonator or a delay line as the frequency selection element. (b) Output spectrum for a single-mode oscillator, and (c) comb-generator.

In this paper, we have demonstrated both the single-mode oscillator and comb generation to fully exploit the advances made in $LiNbO_3$ plate wave ADLs. We use a fabricated SH_0 mode ADL with f_o = 157 MHz, IL = 2.9 dB, τ_G = 270 ns, and FBW > 6% as the demonstration vehicle [6]. Two commercially available low noise RF amplifiers are used to configure oscillator circuits with variable carrier power. Finally, the oscillator performance is evaluated based on phase noise and dc-current consumption. The demonstrated $LiNbO_3$ ADL oscillators not only outperform the Lamb wave ADL oscillator reported in the literature [12] but also attaining competitive performance to commercial power-consuming SAW ADL oscillators at reduced carrier power [16][17].

ADL-BASED OSCILLATORS

Phase Noise Model

To understand the design parameters of ADL-based oscillators, a linear time-invariant (LTI) phase noise model [18] is adopted in this work. Fig. 1 shows the block diagram of a general feedback oscillator using a high-Q resonator or a delay line as the frequency-determining element. Fig. 1(b) and (c) show the conceptual output spectrum of a single-mode oscillator and a comb generator based on different feedback elements, respectively. Unlike a high-Q resonator providing only one operating point for meeting the Barkhausen criteria, the delay line-based oscillator can operate at different modes within its bandwidth [18]. Under

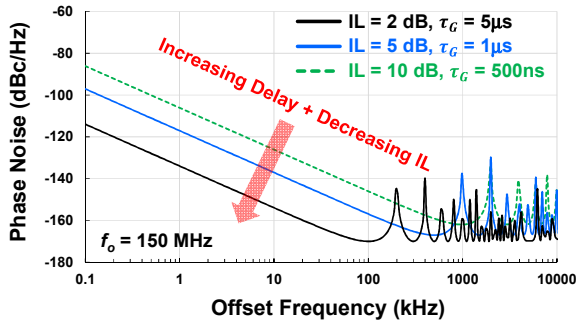

Figure 2: Simulated phase noise for a 150 MHz ADL oscillator with respect to IL and delay based on the model in Fig. 1.

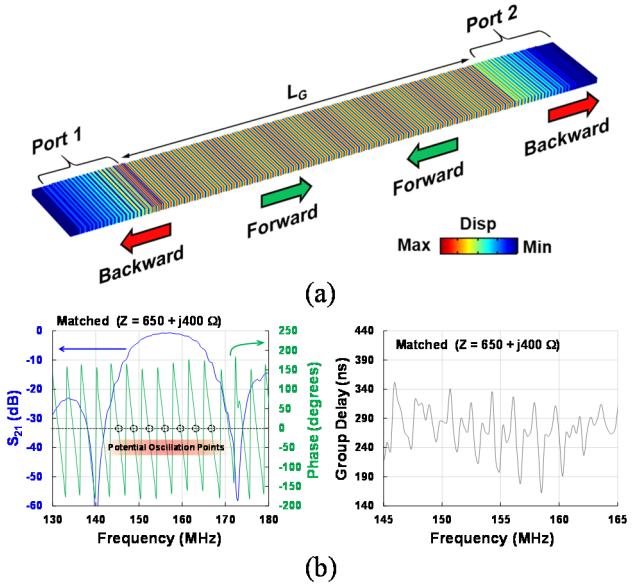

Figure 3: Finite-element-simulated (a) unscaled cross-sectional displacement plot and (b) frequency domain responses of the SH_0 ADL.

multimode oscillation, the spacing between the adjacent modes is inversely proportional to the delay time (τ_G) of the delay line [Fig. 1(c)].

To derive the phase noise, the bandpass response of the ADL is firstly modeled as a delay element with a passband and a time constant $\tau_B = 2Q_{BW}/\omega_o$ [18], and is given by

$$\beta(s) = e^{-s\tau_G} \cdot \frac{1}{1 + s\tau_B}, \tag{1}$$

where $Q_{BW} = \omega_o/\mathrm{BW_{3dB}}$ is derived from the 3 dB bandwidth of the ADL [Fig. 1(a)]. Assuming that the flicker noise in each component can be neglected, the overall phase noise spectrum can then be found in the following form,

$$\mathcal{L}(f_m) \approx 10^{-174-P_C+\mathrm{IL}+\mathrm{NF}} \cdot |H(f_m)|^2 \tag{2}$$

where

$$|H(f_m)|^2 = \frac{1 + f_m^2\tau_B^2}{2 - 2\cos(f_m\tau_G) + f_m^2\tau_B^2 + 2f_m\tau_B\sin(f_m\tau_G)}, \tag{3}$$

and f_m (Hz) is the offset frequency from the carrier, P_C (dBm) is the carrier power in the loop, IL (dB) is the insertion loss of the ADL, and NF (dB) is the noise figure

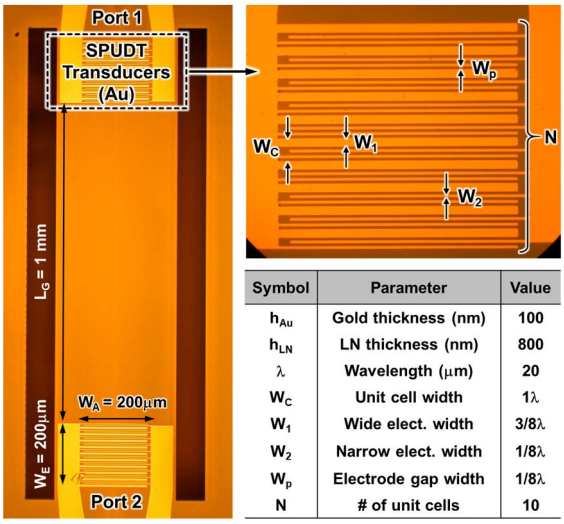

Symbol	Parameter	Value
h_{Au}	Gold thickness (nm)	100
h_{LN}	LN thickness (nm)	800
λ	Wavelength (µm)	20
W_c	Unit cell width	1λ
W_1	Wide elect. width	3/8λ
W_2	Narrow elect. width	1/8λ
W_p	Electrode gap width	1/8λ
N	# of unit cells	10

Figure 4: Optical photo of the fabricated SH_0 ADL with dimensions listed in the table.

of the amplifier, respectively. Fig. 2 depicts the phase noise plots under different IL and delay conditions using the phase noise model. It is evident that *large delay* and *low IL* are the keys to obtain low phase noise based on theoretical modeling.

Design of SH_0 ADL

In this work, the ADL is designed in an X-cut suspended $LiNbO_3$ thin film (800-nm) with thin Au electrodes (100-nm). A pair of single-phase unidirectional transducers (SPUDT) is arranged on the opposite ends of ADL to transmit and receive the SH_0 acoustic wave signal with minimal loss. To obtain the maximum electromechanical coupling coefficient of SH_0, the elastic wave propagation direction is selected at -10° to the +Y axis. Fig. 3(a) illustrates the 3D finite-element displacement plot of the ADL with COMSOL Multiphysics. The delay length L_G between two SPUDTs is set as 1 mm, yielding a moderate time delay around 270 ns. Ten SPUDT cells are selected to obtain low IL and wide bandwidth concurrently for both the single-mode oscillator and comb-generator demonstration. Fig. 3(b) shows the simulated frequency response of the SH_0 ADL in terms of magnitude and phase of S_{21} and extracted group delay. Under conjugate matching, the simulated transmission spectrum shows a wide bandwidth of around 10%. Minor ripples in extracted group delay [Fig. 3(b)] are caused by the finite unidirectionality of the transducers and internal multi-reflections [8]. More importantly, there are seven potential oscillation points within ADL passband due to the long delay around 270 ns.

The MEMS ADL is fabricated based on the process described in [6]. The gold electrodes are well protected by the photoresist (PR) from being exposed to XeF_2 during the device release step. Finally, Fig. 4 shows the optical photo of the fabricated SH_0 ADL with its dimensions labeled.

EXPERIMENTAL RESULTS

ADL Characterization and Oscillator Design

The fabricated SH_0 ADL is characterized by the Keysight PNA-X N5249A vector network analyzer. The

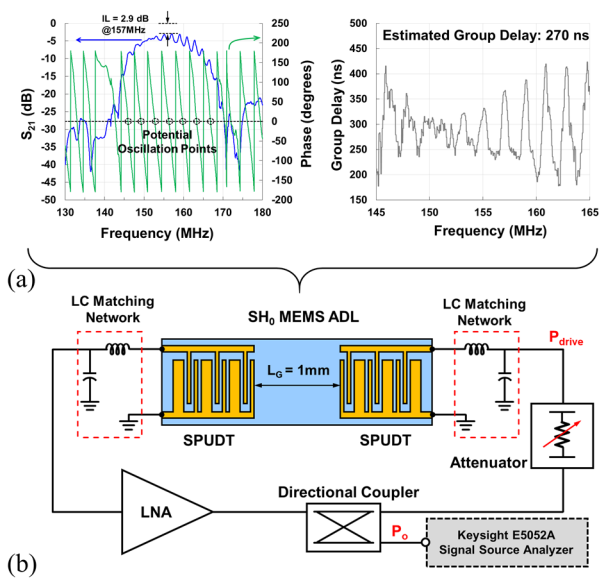

Figure 5: (a) Open-loop characterization of the SH_0 ADL with matching network integrated on PCB. (b) Circuit topology of the ADL-based oscillator.

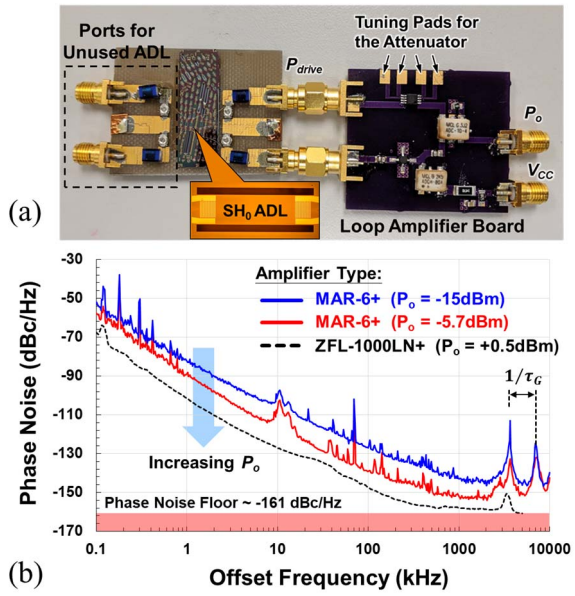

Figure 6: (a) Oscillator board photo with MAR-6+ as the feedback amplifier. (b) Measured phase noise plots under different carrier power levels.

ADL is matched to 50 Ω ports of the PNA using tunable LC matching networks on the printed circuit board (PCB), revealing a minimum IL of 2.9 dB at 157 MHz, as shown in Fig. 5(a). The extracted group delay shows larger ripples spanning from 200 to 440 ns than the simulation results in Fig. 3(b), producing an averaged τ_G near 275 ns.

Fig. 5(b) presents a detailed oscillator circuit schematic. In this work, a specific ADL on the MEMS chip is paired with two low noise amplifiers (MAR-6+ and ZFL-1000LN+ from Mini-Circuits, Inc.). Both amplifiers feature similar NF below 2.9 dB. The MAR-6+ is biased at a lower supply voltage (V_{CC} = 6 V) for lower carrier power operation. Instead, ZFL-1000LN+ is operated at V_{CC} = 15 V for larger carrier power. The variable attenuator is placed before ADL as a passive limiter for tuning the driving power (P_{drive}).

Measurement Results

Fig. 6(a) shows the photo of the evaluation board with MAR-6+ as the amplifier. Fig. 6(b) presents the measured phase noise under various output power (P_o). By changing the attenuation, three phase noise curves with different carrier power levels are recorded. With MAR-6+, the phase noise of -99 dBc/Hz and -109 dBc/Hz at 10-kHz offset are measured under P_o = -15 dBm and -5.7 dBm, respectively. In this configuration, the LNA is intended to deliver low output power because of its low supply voltage (V_{CC} = 6V). By replacing the LNA with ZFL-1000LN+, phase noise of -127 dBc/Hz is measured at 10-kHz offset with P_o = 0.5 dBm. Since the NFs of both LNAs are similar, higher carrier power leads to better phase noise at all offsets as expected. The minimum phase noise floor demonstrated in this work is lower than -161 dBc/Hz.

We also have studied the phase noise behavior under large carrier power with LNA ZFL-1000LN+. The output power P_o is measured from the output terminal of the directional coupler within the attenuation range from 20 dB to 5 dB, as shown in Fig. 7(a). Initially, the phase noise

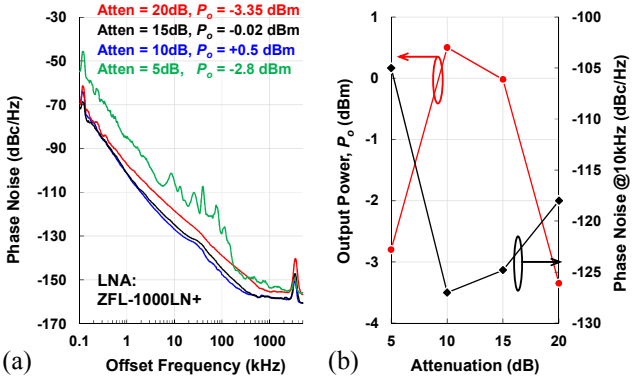

Figure 7: (a) Overall phase noise variations and (b) output power and phase noise at 10-kHz offset with respect to different attenuation.

improves as the attenuation decreases due to the increased P_o. However, as the attenuation goes from 10 dB to 5 dB, the phase noise worsens and P_o reduces from 0.5 to -2.8 dBm. This phenomenon is likely related to the temperature rise of the delay line at higher power. The relationship between P_o and phase noise at 10-kHz offset is summarized in Fig. 7(b).

Finally, the frequency comb generation is also demonstrated using ZFL-1000LN+ with proper biasing conditions, as shown in Fig. 8(a). The comb spacing of 3.4 MHz matches the simulation results in Fig. 3(b) as well as the open-loop characterization in Fig. 5(a). The phase noise of the comb generator is depicted in Fig. 8(b).

Comparisons between this work and previous arts are tabulated in Table 1, confirming that the demonstrated oscillator has a comparable phase noise but with wider bandwidth and lower supply current consumption. Finally, the close-to-carrier phase noise is limited by the insufficiently long delay and the flicker noise of the system. Provide with minimized propagation loss in ADLs [7][8], there is still great potential for further improvement in ADL oscillators.

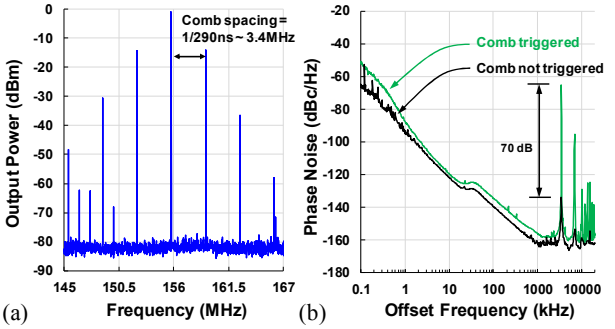

Figure 8: Demonstration of comb generation using ZFL-1000LN+. (a) Wideband oscillation spectrum. (b) Phase noise comparison of the single-mode oscillator and comb generator.

Table 1: Comparison of Single-Mode ADL Oscillators.

References	[12]	[16]	[17]	This work	
Material	GaN	GaN on Si	Quartz	$LiNbO_3$	
Device Type	Delay Line Narrow Band	Delay Line Narrow Band	Delay Line Narrow Band	Delay Line Wide Band	
Acoustic Mode	A_0 Lamb	SAW	SAW	SH_0	
Frequency (MHz)	59.7	252	622	157	
DL Bandwidth (MHz)	–	~0.252* (0.1%)	1.3 (0.2%)	10 (6.45%)	
Insertion Loss (dB)	30.2	28.2	10	3.2	
Delay Time (ns)	–	–	–	200 – 440 (Estimated: 270)	
Power Supply Current, I_{CC} (mA)	40*	40*	65	16 (MAR-6+)	48 (ZFL-1000LN+)
Max. Output Power, P_{o_max} (dBm)	15.1	5.2	13	-5.7**	0.5**
PN @1-kHz (dBc/Hz)	-80	–	-109	-90	-101
PN @10-kHz (dBc/Hz)	-120	–	-132	-109	-127
PN Floor (dBc/Hz)	-150 @10-MHz	-105 @300-kHz	-165 @10-MHz	-153 @1-MHz	-161 @ 5-MHz

* Extracted from the Q-factor * The custom GaN amplifiers used in [12] and [16] are the same
** Including the coupling loss of ~10 dB from the directional coupler

CONCLUSION

We have presented the design and characterization of the single-mode RF oscillators as well as a comb generator based on a thin-film SH_0 $LiNbO_3$ ADL at 157 MHz. The oscillator shows phase noise of -109 dB/Hz at 10-kHz and -153 dBc/Hz at 1-MHz offset at a carrier frequency of 157 MHz while consumes only 16 mA. The acoustic comb generation has also been demonstrated with the same delay line under proper biasing conditions. The demonstrated $LiNbO_3$ ADL oscillator is comparable to the published SAW and Lamb-wave ADL oscillators in terms of phase noise and current consumption.

ACKNOWLEDGMENTS

The authors would like to thank the DARPA NZero program, the NSF SpecEES program (Grant 1824320) and the Young Scholar Fellowship Program of Ministry of Science and Technology of Taiwan (MOST 108-2636-E-007-014) for funding support.

REFERENCES

[1] H. Wohltjen, A. W. Snow, W. R. Barger and D. S. Ballantine, "Trace chemical vapor detection using SAW delay line oscillators," *IEEE Trans. Ultrason. Ferroelect. Freq. Contr.*, vol. 34, no. 2, pp. 172-178, Mar. 1987.

[2] R. Lu, T. Manzaneque, Y. Yang, L. Gao, A. Gao, and S. Gong, "A radio frequency nonreciprocal network based on switched acoustic delay lines," *IEEE Trans. Microw. Theory Techn.*, vol. 67, no. 4, pp. 1516– 1530, 2019.

[3] L. Eichinger, F. Sischka, G. Olbrich and R. Weigel, "Accurate design of low-noise microwave SAW oscillators," in *Proc. IEEE Ultrason. Int. Symp.*, Oct. 2000, pp. 29-34.

[4] R. H. Tancrell and M. G. Holland, "Acoustic surface wave filters," *Proc. IEEE*, vol. 59, no. 3, pp. 393–409, 1971.

[5] C. Campbell, *Surface Acoustic Wave Devices and Their Signal Processing Applications*. Academic Press, 1989.

[6] T. Manzaneque, R. Lu, Y. Yang, and S. Gong, "Low-loss and wideband acoustic delay lines," *IEEE Trans. Microw. Theory Techn.*, vol. 67, no. 4, pp. 1379–1391, Apr. 2019.

[7] R. Lu, T. Manzaneque, Y. Yang, M.-H. Li, and S. Gong, "Gigahertz low- loss and wide-band S0 mode lithium niobate acoustic delay lines," *IEEE Trans. Ultrason. Ferroelect. Freq. Contr.*, vol. 66, no. 8, pp. 1373–1386, 2019.

[8] R. Lu, Y. Yang, M.-H. Li, T. Manzaneque, and S. Gong, "GHz broadband SH0 mode lithium niobate acoustic delay lines," *IEEE Trans. Ultrason. Ferroelect. Freq. Contr.*, In Press.

[9] G. Vidal-Alvarez, A. Kochhar, and G. Piazza, "Delay line with different receiver-resonator channels as an all mechanical front-end of a discrete matched filter for wake-up radios," *IEEE Int. Conf. Micro Electro Mech. Syst.*, Jan. 2018, pp. 162-165.

[10] R. H. Olsson III *et al.*, "A high electromechanical coupling coefficient SH0 Lamb wave lithium niobate micromechanical resonator and a method for fabrication," *Sens. Actuators A-Phys.*, vol. 209, pp. 183–190, Mar. 2014.

[11] R. Lu, S. Link, S. Zhang, M. Breen, and S. Gong, "Aluminum nitride Lamb wave delay lines with sub-6 dB insertion loss," *J. Microelectromech. Syst.*, vol. 28, no. 4, pp. 569-571, Aug. 2019.

[12] X. Lu, J. Ma, C. P. Yue, and K. M. Lau, "A GaN-based Lamb-wave oscillator on silicon for high-temperature integrated sensors," *IEEE Microw. Wireless Compon. Lett.*, vol. 23, no.6, pp.318–320, June 2013.

[13] H. Zhu and M. Rais-Zadeh, "Switchable Lamb wave delay lines using AlGaN/GaN heterostructure," in *2017 19th International Conference on Solid-State Sensors, Actuators and Microsystems (TRANSDUCERS)*, Kaohsiung, 2017, pp. 179-182.

[14] R. Lu, T. Manzaneque, Y. Yang, M.-H. Li, and S. Gong, "Towards digitally addressable delay synthesis: GHz low-loss acoustic delay elements from 20 ns to 900 ns," in *IEEE Int. Conf. Micro Electro Mech. Syst.*, Jan. 2019, pp. 121-124.

[15] I. D. Avramov and Z. G. Georgiev, "A surface-acoustic-wave comb spectrum oscillator for sensor applications," *IEEE Trans. Ultrason. Ferroelect. Freq. Contr.*, vol. 38, no. 4, pp. 334-336, July 1991.

[16] X. Lu, J. Ma, X. L. Zhu, C. M. Lee, C. P. Yue, and K. M. Lau, "A novel GaN-based monolithic SAW/HEMT oscillator on silicon," in *Proc. IEEE Ultrason. Int. Symp.*, Oct. 2012, pp. 2206-2209.

[17] Integrated Device Technology, Inc., "IDT White Paper: Voltage Controlled SAW Oscillator (VCSO) Fundamentals." [Online] Available: https://www.idt.com/document/whp/voltagecontrolledsawosc-vcso-fundamentals

[18] E. Rubiola, *Phase noise and frequency stability in oscillators*. Cambridge, U.K.: Cambridge Univ. Press, 2008.

CONTACT

*M.-H. Li, mhli@pme.nthu.edu.tw